

Supporting Information

Highly ordered mesoporous carbon nanofiber arrays from a crab shell biological template and its application in supercapacitors and fuel cells

Hai-Jing Liu, Xiao-Ming Wang, Wang-Jun Cui, Yu-Qian Dou, Dong-Yuan Zhao,
Yong-Yao Xia*

Department of Chemistry and Shanghai Key Laboratory of Molecular Catalysis and Innovative Materials, Institute of New Energy, Fudan University, Shanghai 200433 (P. R China)
E-mail: yyxia@fudan.edu.cn

Figures and Results

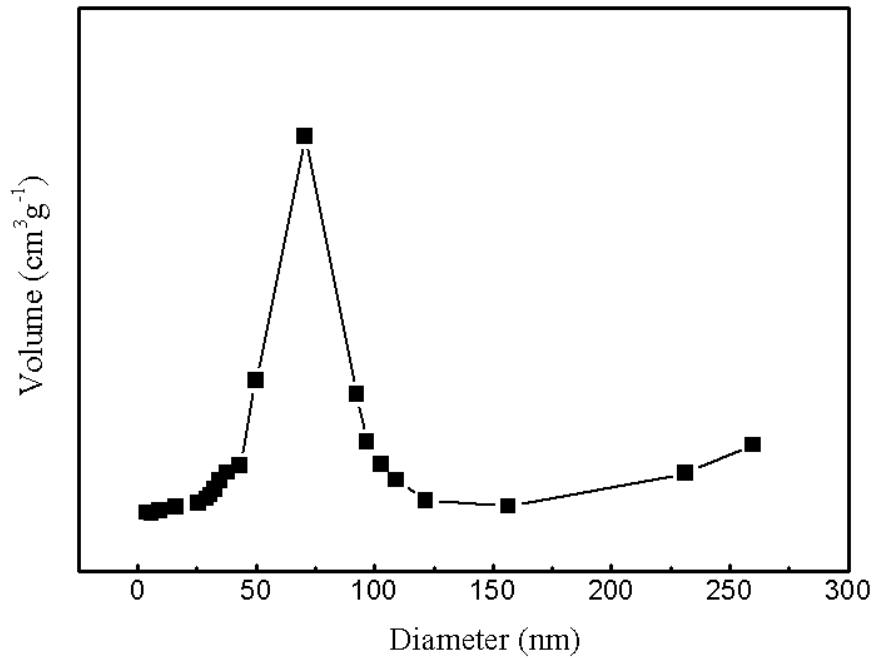


Figure S1 Pore-size distribution calculated from the N₂ sorption isotherms of the crab shell template.

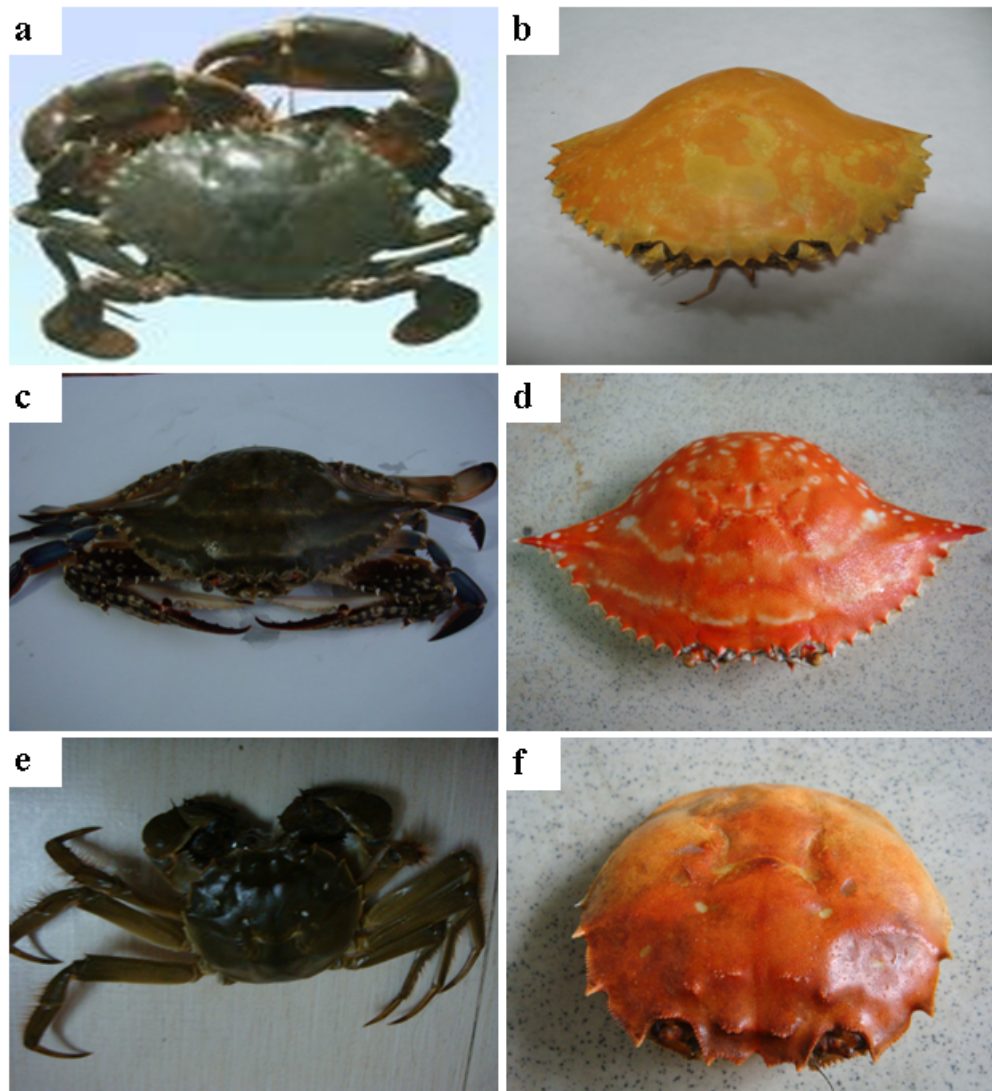


Figure S2 Three kinds of crabs and their shells and shells after calcination in air at 350 °C, which live in different environments. (a) and (b), *scylla serrata* crab; (c) and (d), portunid crab; (e) and (f), hairy crab.

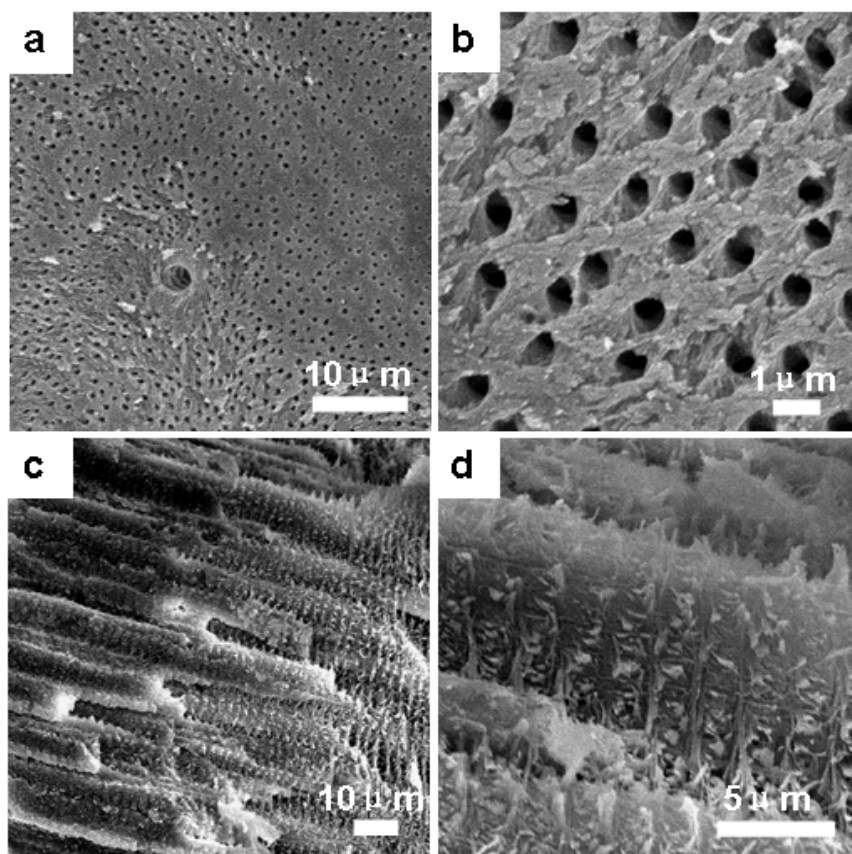


Figure S3 SEM images of portunid crab shell template. (a) and (b), top-view images; (c) and (d), side-view images.

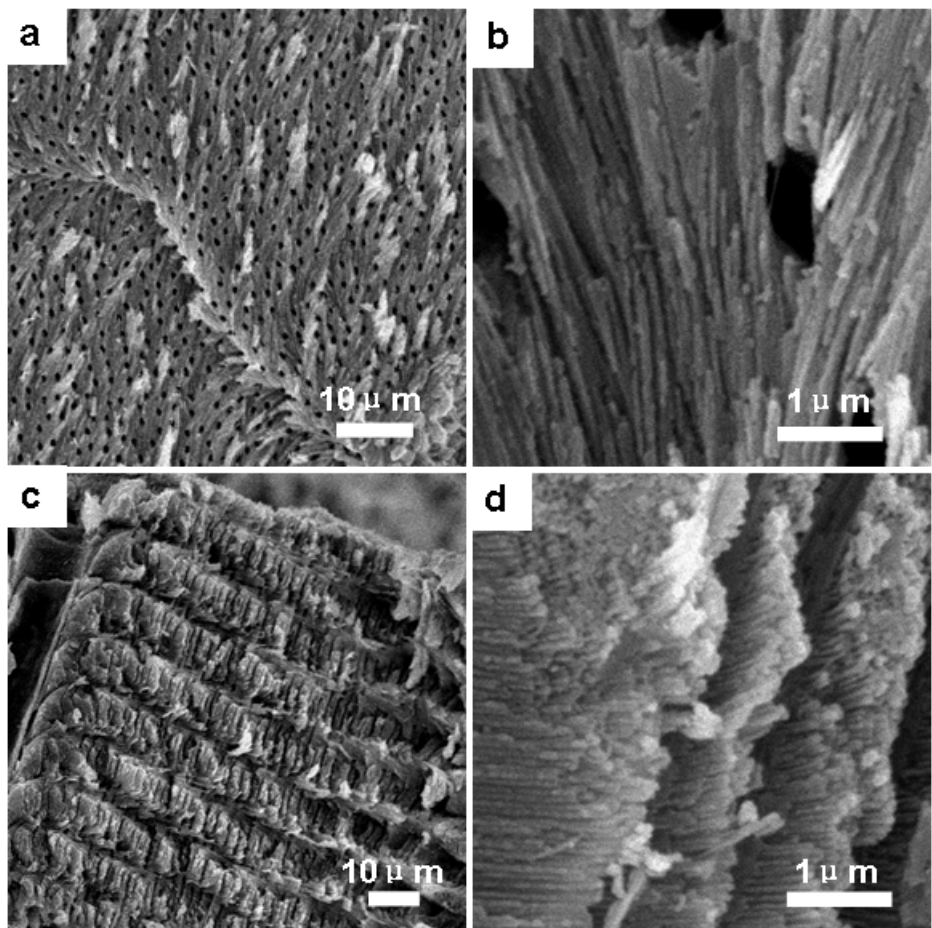


Figure S4 SEM images of hairy crab shell template. (a) and (b), top-view images; (c) and (d), side-view images.

Fig. S2 shows photographs of the three crabs and their shells, which live in different environments: the scylla serrata crab lives in shallow seas (Fig. S2 (a) and S2 (b)), the portunid crab lives in the deep seas (Fig. S2 (c) and S2 (d)) and the hairy crab lives in rivers (Fig. S2 (e) and S2 (f)). The SEM images of the portunid crab and the hairy crab are shown in Fig. S3 and S4. We found that most crab shells showed very similar structures despite their different living environments. The differences may influence the interlaced array structure and the pore-to-pore distance.

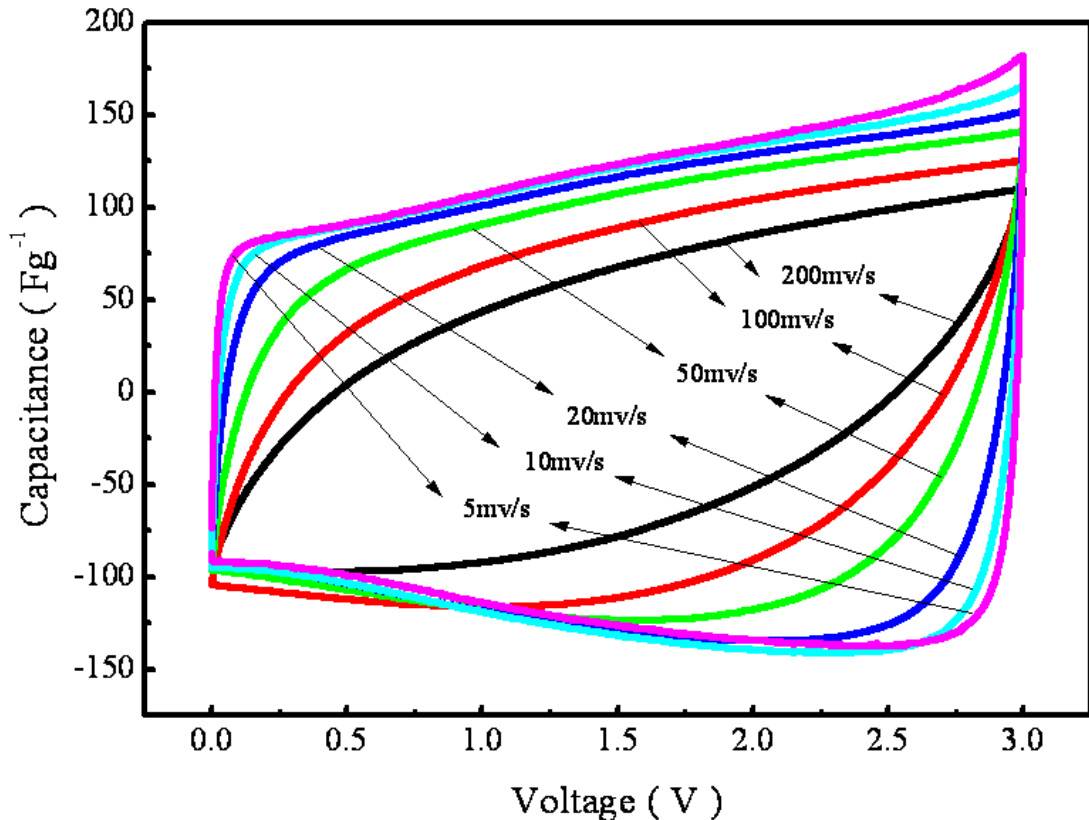


Figure S5 The CV profiles of AC. Investigated at different scan rates from 5 to 200 mVs⁻¹ between 0 and 3 V in 1 M (C₂H₅)₄NBF₄/PC electrolyte using a two-electrode quasi-capacitor.

Fig. S5 shows the CV profiles of AC investigated at different scan rates from 5 mVs⁻¹ to 200 mVs⁻¹ between 0 and 3 V in 1 M (C₂H₅)₄NBF₄/PC electrolyte using a two-electrode quasi-capacitor. The capacitance of the carbon material can be estimated by the equation of $C = 2i/v$, where C is the differential capacitance and i is the current density; in this case, the value of 1.5 V was chosen and v is the scan rate, all multiplied by 2 because the two carbon electrodes of the capacitor are actually connected in series. It is well-known that the steepness in the current change at the switching potential is determined by the resistance and capacitance time (RC)

constant. The nearly 90° change in the CV curve at the switching potential indicates that the MCNAs has a very small time constant as an ideal capacitor. The calculated capacitance of AC was 127 Fg⁻¹. Considering the differences in surface area, the specific surface area capacitance of MCNAs was 12 µFcm⁻¹, which is 2 times higher than that of commercial AC (about 6 µFcm⁻¹). It is most interesting to clarify the issues as to why there is such a significant difference in the capacitance between these two carbon materials. The pore diameter of AC was estimated to be 2.2 nm according to the nitrogen sorption measurements. However, a large proportion of the micropore area, about 477 m²g⁻¹, nearly 23 % of the total surface area (2071 m²g⁻¹), was detected. Similar results were also reported in Ref 3. It has been demonstrated that the very narrow micropores do not contribute to the total double layer capacitance because of a molecular sieving effect,^{S1-S3} thus decreasing the utilization of specific surface area. Aside from the pore size distribution, it is well-recognized that the pore shape, the surface functional groups, the electrolyte accessibility, the solvated-ion effect and the electronic conductivity can be critical to the electrical double layer performance. It is probable that the pore texture and surface properties of the AC in the present work would not be favorable for the penetration of electrolyte and ion transportation at high scan rates. We speculate that most of the surface area in the AC is difficult for non-aqueous electrolyte wetting when using a high scan rate, thus giving rise to a decrease in capacitance. For the MCNAs, its larger pore size and large channels between nanofibers benefit electrolyte immersion, and also a very low micropore area contributes (72 cm²g⁻¹) to the total surface area.

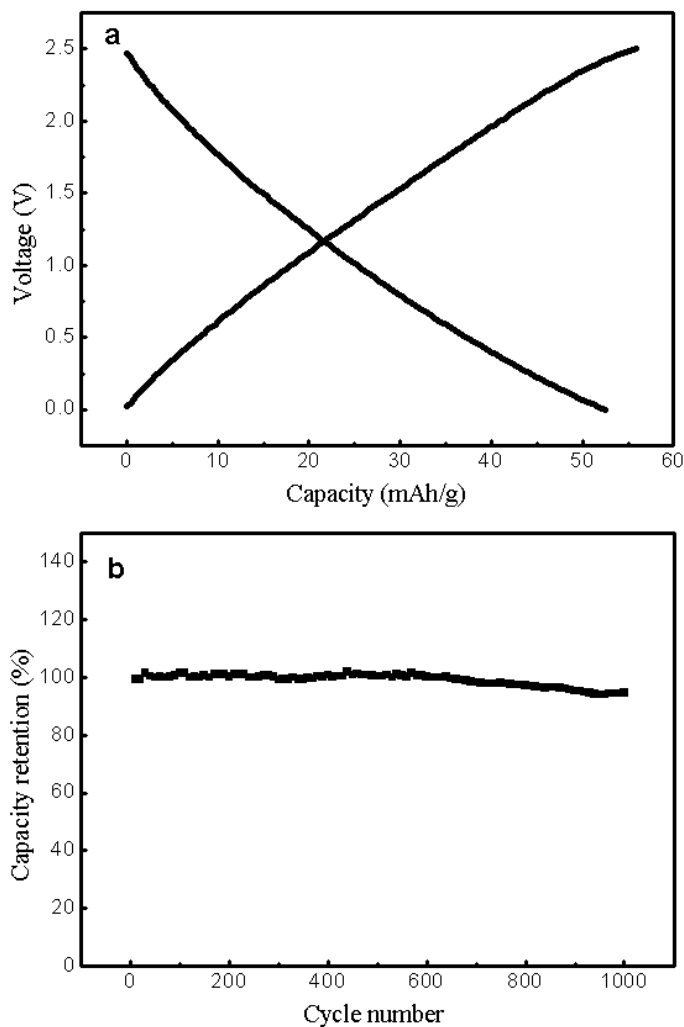


Figure S6 Capacitive performances of MCNAs. (a), Galvanostatic charge/discharge curves of the MCNAs capacitor at a current density of 100 mA g^{-1} in $1\text{M} (\text{C}_2\text{H}_5)_4\text{NBF}_4/\text{PC}$ electrolyte; (b), cycling performance of MCNAs capacitor. The cell was cycled at a constant current of 500 mA g^{-1} between 0 and 3 V.

Fig. S6 (a) shows the galvanostatic charge/discharge curves of the MCNAs capacitor at a current density of 100 mA g^{-1} in $1\text{M} (\text{C}_2\text{H}_5)_4\text{NBF}_4/\text{PC}$ electrolyte and a perfect capacitive behavior with linear shape characteristics that is observed between 0 and 2.5 V at a current density of 100 mA g^{-1} . The capacity of MCNAs is about 53 mAh g^{-1} based on the mass load of one electrode, corresponding a specific capacitance

of 152 Fg^{-1} . The result is consistent with the value obtained by the CV test. Figure S6 (b) gives the cycle performance of the MCNAs capacitor investigated by charging/discharging the capacitor for 1000 cycles at a current density of 500 mAg^{-1} between 0 and 2.5 V. The MCNAs capacitor maintained 95 % of its initial capacity after 1000 cycles, and the columbic efficiency was maintained at about 95 %.

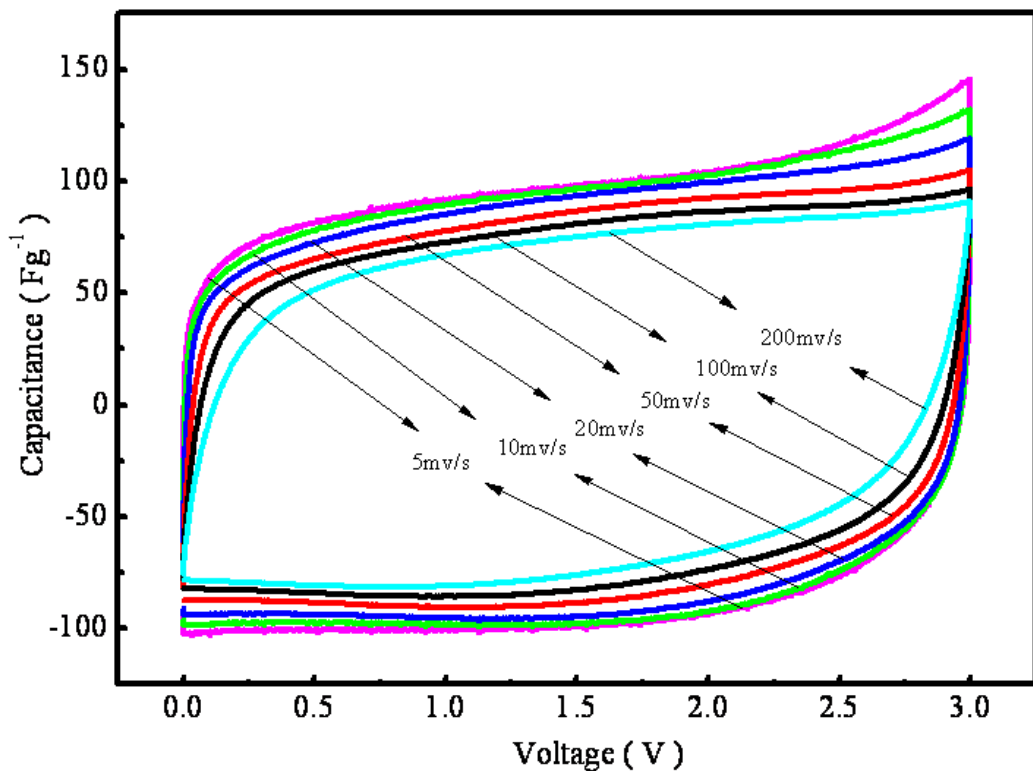


Figure S7 The CV profiles of C (carbon nanofibers from carbonization of phenolic resol precursors after removing crab shell and P123). Investigated at different scan rates from 5 to 200 mVs^{-1} between 0 and 3 V in 1 M $(\text{C}_2\text{H}_5)_4\text{NBF}_4/\text{PC}$ electrolyte using a two-electrode quasi-capacitor.

Table S1: Comparison of catalytic properties of the catalysts

catalyst	Onset potential (V vs.SCE)	I_f (mA cm^{-2})	Peak potential (V vs.SCE)	I_b (mA cm^{-2})	I_f/I_b
Pt/MCNAs	0.224	10.82	0.645	9.05	1.20
Pt/XC72R	0.305	6.83	0.649	8.14	0.84

I_f and I_b are corrected for electric double-layer capacitance.

Methanol electrooxidation on Pt/MCNAs and Pt/XC72R electrodes was compared in the following areas to indicate the catalytic performance: onset potential of methanol oxidation, forward peak potential, forward peak current density, and ratio of the forward peak current density (I_f) to the backward peak current density (I_b). According to the CV profiles, the above particulars are listed in Tab. S1. The onset potential and peak potential of methanol electrooxidation on Pt/MCNAs shift negatively by 81 mV and 4mV respectively, accompanied by nearly 60 % increase in the forward peak current density. Moreover, it is notable that I_f/I_b significantly increases. Goodenough et al. attributed this anodic peak (I_b) in the reverse scan to the removal of the incompletely oxidized carbonaceous species formed in the forward scan.^{S4} These carbonaceous species are mostly in the form of linearly bonded Pt=C=O. Hence the ratio of the forward anodic peak current density (I_f) to the reverse anodic peak current density (I_b), I_f/I_b , can be used to describe the catalyst tolerance to carbonaceous species accumulation. Low I_f/I_b ratio indicates poor oxidation of methanol to carbon dioxide during the anodic scan and excessive accumulation of carbonaceous residues on the catalyst surface. High I_f/I_b ratio shows the converse case.

In a word, Pt supported on MCNAs exhibits a much higher activity than Pt/XC72R for methanol electrooxidation.

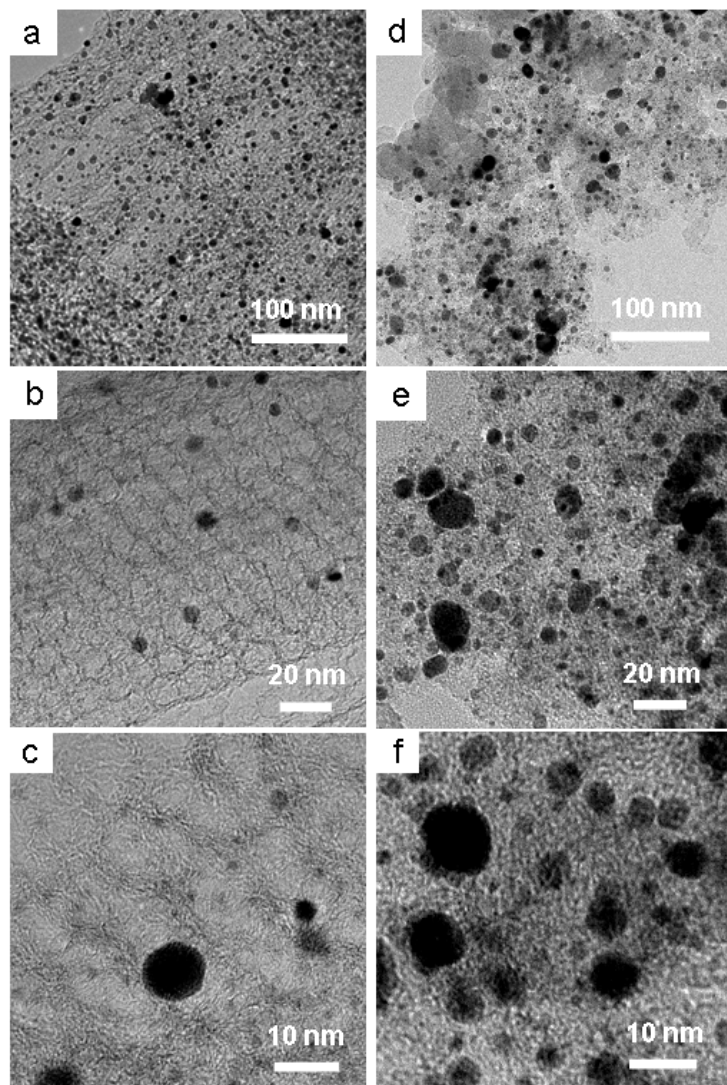


Figure S8 TEM images. (a), (b) and (c), Pt/MCNAs; (d), (e) and (f), Pt/XC72R.

Fig. S8 displays varying catalyst morphologies. Comparison of the TEM images ((a) and (d)) of two catalysts indicates that the Pt nanoparticles of the Pt/MCNAs catalyst are highly dispersed on the MCNAs surface, while the dispersion of the Pt nanoparticles of the Pt/XC72R catalyst on the carbon support is uneven with prevalent

agglomerations. According to TEM image (b) of high resolution, some Pt nanoparticles sit in mesopores, thus restraining their aggregations; others locate on the brim of the mesopore-wall. TEM image (c) further reveals that the mesopore-wall is highly graphitized, which provides plentiful vacancies or defects in a graphite plane of the edge of mesopore-wall. It has demonstrated that vacancies or defects can dissociate H₂O to H and OH species, thus improving the CO oxidation ability. However, XC72R does not possess this microstructure (image (e) and (f)).

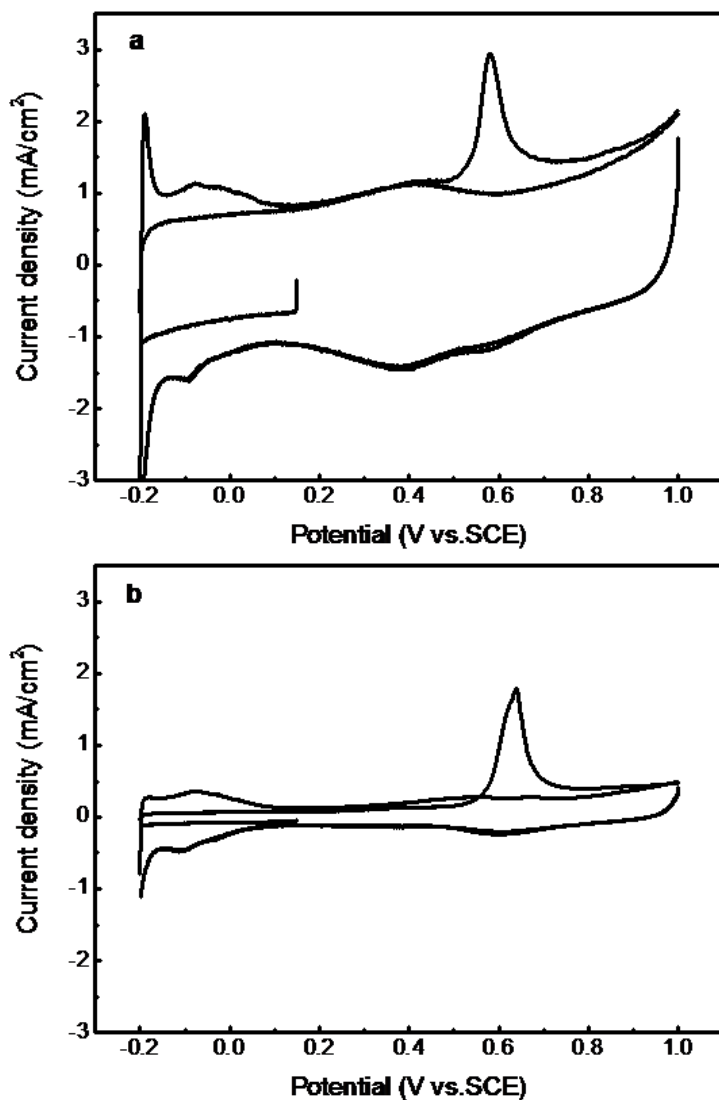
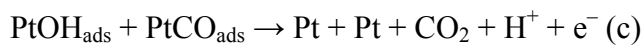


Figure S9 CO-stripping voltammograms in 0.5 M H₂SO₄ + 0.5 M methanol at a scan rate of 20 mVs⁻¹. (a), Pt/MCNAs electrode; (b), Pt/XC72R electrode.

Cyclic voltammograms with and without CO_{ad} on Pt/MCNAs (a) and Pt/XC72R (b) electrodes are showed in Figure S9, and two pieces of information can be revealed. Firstly, the onset potential of CO-stripping on the Pd/MCNAs (a) electrode shifts negatively near 170 mV, investigating significantly accelerating CO oxidation ability of the Pt nanoparticles on MCNAs. Above TEM measurement has proved that there are plentiful vacancies or defects in a graphite plane of MCNAs, which can effectively dissociate H₂O to H and OH species. This process may be promoted by the presence of Pt that acts adsorption and dissociation active sites via spillover effect (eq. c), thus accelerating the CO oxidation. This is in good agreement with the result of I_f/I_b in CV measurement.



Secondly, based on CO-stripping measurement the specific surface area can be calculated. The results are 60.71 m²g⁻¹ and 34.52 m²g⁻¹ respectively, which accords with the results of TEM measuments.

Supporting references

S1 L. Eliad, G. Salitra, A. Soffer and D. Aurbach, *J. Phys. Chem. B*, 2001, **105**, 6880-6887.

S2 G. Salitra, A. Soffer, L. Eliad, Y. Cohen and D. Aurbach, *J. Electrochem. Soc.*, 2000, **147**, 2486-2493.

S3 L. Eliad, G. Salitra, A. Soffer and D. Aurbach, *J. Phys. Chem. B*, 2002, **106**,

10128-10134.

S4 R. Manohara and J. B. Goodenough, *J. Mater. Chem.*, 1992, **2**, 875-887.